Published in final edited form as:
Cancer Discov. 2014 October ; 4(10): 1168–1181. doi:10.1158/2159-8290.CD-13-0747.

A Large-Scale RNAi-Based Mouse Tumorigenesis Screen Identifies New Lung Cancer Tumor Suppressors that Repress FGFR Signaling

Ling Lin[1], **Lynn Chamberlain**[1], **Magnolia L. Pak**[1], **Arvindhan Nagarajan**[2], **Romi Gupta**[2], **Lihua J. Zhu**[3], **Casey M. Wright**[4,5], **Kwun M. Fong**[5], **Narendra Wajapeyee**[2], and **Michael R. Green**[1]

[1]Howard Hughes Medical Institute, Programs in Gene Function and Expression and Molecular Medicine, University of Massachusetts Medical School, Worcester, Massachusetts

[2]Department of Pathology, Yale University School of Medicine, New Haven, Connecticut

[3]Programs in Gene Function and Expression, Molecular Medicine and Bioinformatics and Integrative Biology, University of Massachusetts Medical School, Worcester, Massachusetts

[4]University of Queensland, School of Medicine, Brisbane, Queensland, Australia

[5]Department of Thoracic Medicine, The Prince Charles Hospital and University of Queensland Thoracic Research Centre, Brisbane, Queensland, Australia

Abstract

To discover new tumor suppressor genes (TSGs), we developed a functional genomics approach in which immortalized but non-tumorigenic cells were stably transduced with large-scale short hairpin RNA (shRNA) pools and tested for tumor formation in mice. Identification of shRNAs in resulting tumors revealed candidate TSGs, which were validated experimentally and by analyzing expression in human tumor samples. Using this approach, we identified 24 TSGs that were significantly down-regulated in human lung squamous cell carcinomas (hLSCCs). Amplification of fibroblast growth factor receptor 1 (*FGFR1*), which aberrantly increases FGFR signaling, is a common genetic alteration in hLSCCs. Remarkably, we found that 17 of the TSGs encode repressors of FGFR signaling. Knockdown of 14 of these TSGs transformed immortalized human bronchial epithelial cells and, in most cases, rendered them sensitive to FGFR inhibitors. Our results indicate that increased FGFR signaling promotes tumorigenesis in many hLSCCs that lack FGFR1 amplification or activating mutations.

Keywords

FGFR1 signaling; functional genomics; hLSCC; RNA interference screening; tumor suppressor genes

Corresponding author: Michael R. Green, University of Massachusetts Medical School, 364 Plantation Street, Worcester, MA 01605. Phone: 508-856-5330; Fax: 508-856-5473; michael.green@umassmed.edu.

The authors disclose no potential conflicts of interest.

Disclosure of Potential Conflicts of Interest
No potential conflicts of interest were disclosed by the authors.

INTRODUCTION

A goal of contemporary cancer research is to identify all genes responsible for neoplastic transformation. For example, the identification of new TSGs has important implications for both diagnosing and treating cancer. One of the ongoing efforts to identify the genes responsible for tumor formation is partial or complete sequencing of cancer genomes (reviewed in (1)). Although this approach has and will continue to reveal genes involved in tumorigenesis, there are specific challenges for discovery of TSGs solely by sequence analysis of cancer genomes. First, the genomes of cancer cells are error-prone (reviewed in (2)) and thus many of the mutations found in cancer cells are not causally related to the transformed phenotype. Second, in many instances TSGs are inactivated by transcriptional repression (commonly referred to as epigenetic silencing) rather than a mutational event, and thus would not be identified by conventional genome-sequencing methods. Transcriptionally silenced TSGs bear several hallmarks including repressive histone modifications and hypermethylated CpG-rich promoter regions (reviewed in (3)).

Functional genomics approaches for TSG discovery are highly complementary to cancer genome sequencing efforts. Here we describe and demonstrate a large-scale RNA interference-based functional screen for TSG discovery.

RESULTS

A Large-Scale shRNA Screen Identifies Candidate TSGs

To identify TSG candidates, we performed a large-scale shRNA screen for tumorigenesis in mice, which is summarized in Fig. 1A and discussed below. We used mouse NIH 3T3 fibroblasts, which are immortalized but not transformed and can be rendered tumorigenic by a wide range of oncogenic events (see, for examples, (4–7)). We first performed a reconstruction experiment to determine the minimal number of transformed NIH 3T3 cells required for tumorigenesis. Toward this end, 1000, 100 or no *Kras*-transformed NIH 3T3 cells were added to 1×10^6 non-transformed NIH 3T3 cells and injected into the flanks of nude mice. Figure 1B shows that 100 transformed NIH 3T3 cells (and likely fewer) are sufficient for detectable tumor formation.

For the primary screen, a genome-wide mouse shRNA library comprising 62,400 shRNAs (8) was divided into 10 pools, which were packaged into retrovirus particles and used to stably transduce NIH 3T3 cells. For each of the 10 stable cell populations, 1×10^6 cells were injected subcutaneously into the flank of a nude mouse. Thus, each of the 6240 shRNAs in each pool was present in ~160 cells, which is greater than the 100 *Kras*-transformed NIH 3T3 cells that enabled tumor formation. We found that seven of the ten shRNA pools gave rise to detectable tumors. After two weeks, tumors were dissected and genomic DNA was extracted. To identify the candidate shRNAs, the shRNA region of the transduced virus was PCR amplified, cloned and sequenced. In total, 39 independent shRNAs were recovered from the seven tumors.

To validate the candidates, single shRNAs directed against each gene were stably transduced into NIH 3T3 cells to derive NIH 3T3 knockdown cell lines. Quantitative real-time RT-PCR (qRT-PCR) confirmed in all cases that expression of the target gene was decreased in the corresponding NIH 3T3 knockdown cell line (Supplementary Fig. S1A). We then tested the ability of the NIH 3T3 knockdown cells lines to form tumors following subcutaneous injection into nude mice. Figure 1C shows that 32 of the 39 shRNAs promoted tumor formation. We also tested the ability of the NIH 3T3 knockdown cells lines to form colonies in soft agar. As expected, knockdown of all 32 genes markedly increased anchorage-independent growth (Supplementary Fig. S1B).

For all 32 genes a second, unrelated shRNA directed against the same target gene also promoted colony formation in soft agar (Supplementary Fig. S1C) and decreased expression of the target gene (Supplementary Fig. S1D), ruling out off-target effects. For 17 of the genes that we analyze in greater detail below, we also tested the ability of a second, unrelated shRNA to promote tumor formation in mice. In all 17 cases, knockdown of the TSG with the second shRNA also resulted in tumor formation (Supplementary Fig. S1E). Of the 32 candidate TSGs, unambiguous human homologs could be identified in 28 cases (Table 1). Significantly, several of the genes such as *IGF2R* (9), *SEMA3B* (10), and *STK11* (also known as *LKB1*) (11) are well documented TSGs, validating the overall experimental strategy.

Many Candidate TSGs are Down-Regulated in hLSCC Samples

To gain insight into the tumor types in which the candidate TSGs may play a role, we queried the Oncomine cancer profiling database (12). Notably, a large fraction of the candidate TSGs were down-regulated in lung cancers (Supplementary Table S1). To confirm and extend this finding, we analyzed expression of the 28 genes in a series of hLSCC, lung adenocarcinoma and normal lung samples. The results of Fig. 2A and Supplementary Fig. S2 show that 24 of the 28 candidate TSGs were down-regulated greater than 2-fold in ≥70% of the hLSCC samples analyzed. By contrast, only five candidate TSGs were down-regulated greater than 2-fold in ≥70% of the lung adenocarcinoma samples (Fig. 2B and Supplementary Fig. S3). Consistent with our results, eight candidate TSGs (*DAPP1*, *GZMA*, *IGF2R*, *NAA38*, *NME4*, *NUP205*, *SDF2L1* and *STK11*) are located in the deletion peak datasets of a recent hLSCC genomic characterization study (13).

TSG Promoter Hypermethylation in hLSCC Samples

To determine whether TSG down-regulation was a result of epigenetic silencing, we analyzed promoter DNA methylation in paired primary hLSCC and normal lung squamous cell samples from 18 individuals. For each sample, genomic DNA was isolated, subjected to bisulfite conversion, and hybridized to an Illumina Infinium genome-wide DNA methylation array (14). We then interrogated 26 of the TSGs (*GAPVD1* and *PKD1L3* were absent from the array) against the whole genome dataset. Of the 26 TSGs analyzed, nine displayed a statistically significant increase in promoter hypermethylation in hLSCCs relative to normal samples (Supplementary Fig. S4A–B and Supplementary Table S2). Notably, two of the nine genes, *PTGIS* and *SEMA3B*, are known to be significantly hypermethylated in lung cancers (15–18), validating the methylation analysis. Moreover, of the nine TSGs that we

found to be hypermethylated, six were also recently reported to be hypermethylated in hLSCCs (13). These results indicate that epigenetic silencing due to promoter hypermethylation is one—but not the only—mechanism by which the TSGs are down-regulated in hLSCCs.

Many of the TSGs Encode Repressors of FGFR Signaling

A common genetic alteration in hLSCC is amplification of *FGFR1*, which results in aberrant activation of FGFR signaling (19, 20). We therefore hypothesized that some of the candidate TSGs might function as hLSCC tumor suppressors by repressing FGFR signaling. We first asked whether repressors of FGFR signaling could be isolated in our primary screen by testing whether increased FGFR signaling would render NIH 3T3 cells tumorigenic. Figure 3A shows that NIH 3T3 cells ectopically expressing FGFR1 formed a tumor following subcutaneous injection into a nude mouse, consistent with a previous report that FGFR1 can transform NIH 3T3 cells (21).

We next asked whether knockdown of each TSG (Supplementary Fig. S5A) resulted in increased FGFR signaling. These experiments were performed in SA cells, an immortalized but non-transformed line of human bronchial epithelial cells (HBECs) (22). We first monitored the level of FRS2, a downstream effector that is phosphorylated upon FGFR activation. Remarkably, knockdown of 17 of the 24 TSGs resulted in increased levels of phosphorylated FRS2-Y436 (pFRS2-Y436) relative to that obtained with a non-silencing shRNA control, indicative of increased FGFR signaling (Fig. 3B and Supplementary Fig. S5B and S5C). Moreover, the level of pFRS2-Y436 in several of the SA knockdown cell lines was comparable to that observed in NCI-H520 cells, an hLSCC cell line containing amplified *FGFR1* (19). Notably, the level of total FRS2 (tFRS2) in these 17 SA knockdown cell lines was not increased. Increased FGFR signaling following knockdown of these 17 TSGs was confirmed using two alternative markers of FGFR signaling, pFRS2-Y196 and phospholipase C-γ (PLC-γ) (Supplementary Fig. S6A and S6B); similar results were obtained with a second, unrelated shRNA (Supplementary Fig. S6C and S6D). We also analysed a representative subset of the 17 TSGs in NIH 3T3 cells, which were used in the primary screen. In all cases analyzed, knockdown of the TSG also resulted in increased FGFR signaling (Supplementary Fig. S6E).

Phosphorylation of FRS2 activates the mitogen-activated protein kinase (MAPK) signaling pathway (23). We therefore monitored the levels of phosphorylated ERK1/2 (pERK1/2) in the 24 SA knockdown cell lines. The results of Fig. 3B show that all of the 17 SA knockdown cell lines with elevated pFRS2 also had increased pERK1/2 levels. Interestingly, of the seven SA knockdown cell lines that had normal pFRS2 levels, six had increased pERK1/2 levels (IGF2R, NAA38, MAP1A, PIGH, SEMA3B and ZNF22), indicative of FGFR-independent activation of the MAPK pathway. Consistent with our results, IGF2R (24, 25) and SEMA3B (26) are known to negatively regulate MAPK signaling through an FGFR-independent pathway.

For the 17 SA knockdown cell lines with elevated pFRS2, we analyzed the levels of phosphorylated and total FGFR1 (pFGFR1 and tFGFR1, respectively) to delineate the step in the FGFR signaling pathway that is repressed. The results of Fig. 3C show that seven of

these SA knockdown cell lines had increased pFGFR1 and tFGFR1 levels; four had increased pFGFR1 levels but normal tFGFR1 levels; and six had normal levels of pFGFR1 and tFGFR1. For the seven TSGs that affected tFGFR1 levels, we found that in some but not all cases, shRNA-mediated knockdown increased *FGFR1* mRNA levels (Supplementary Fig. S7A and S7B), indicating that some of the TSGs repress *FGFR1* transcription whereas others act post-transcriptionally. Collectively, these results, which are summarized in Supplementary Table S3, indicate that these 17 TSGs repress FGFR signaling by three distinct mechanisms that modulate either tFGFR1 levels, pFGFR1 levels, or FGFR1-independent FRS2 activation.

For the seven TSGs that affected tFGFR1 levels, we investigated specificity by asking whether their knockdown also affected the levels of other FGF receptors (FGFR2, FGFR3 and FGFR4) and growth factor receptors (epidermal growth factor receptor [EGFR] and insulin receptor [IR]). Knockdown of the seven TSGs did not affect the levels of FGFR2, FGFR3, FGFR4, EGFR or IR (Supplementary Fig. S7C and S7D).

Knockdown of FGFR Signaling Repressors Transforms Immortalized HBECs

The hLSCC cell line NCI-H520, which as stated above has amplified *FGFR1*, is highly dependent upon FGFR signaling for viability and proliferation (27). We therefore predicted that ectopic expression of TSGs that encode repressors of FGFR signaling would inhibit proliferation of NCI-H520 cells. We obtained cDNAs for 14 of the 17 TSGs that encode repressors of FGFR signaling and found in all cases that ectopic expression (Supplementary Fig. S8A and S8B) reduced proliferation, as measured in a soft agar colony formation assay (Supplementary Fig. S8C). As expected, the decreased colony formation resulting from ectopic expression of the TSG was counteracted by co-expression of FRS2 (Supplementary Fig. S8D). Also, as expected, ectopic expression of representative TSGs in NCI-H520 cells repressed FGFR signaling, as evidenced by decreased pFRS2-Y436 levels (Supplementary Fig. S8E). By contrast, ectopic expression of the TSGs in *HRAS*-transformed SA cells, which lack FGFR1 amplification and whose growth is not dependent upon FGFR signaling (see below), had no significant effect on colony formation (Supplementary Fig. S8F).

We also selected a representative subset of eight of these 14 TSGs and tested their ability to inhibit tumor growth in mouse xenografts. Retroviral vectors co-expressing green fluorescence protein (GFP) and one of eight TSGs were transduced into NCI-H520 cells, and GFP-positive cells were isolated by fluorescence-activated cell sorting 24 h later and injected subcutaneously into nude mice. Supplementary Fig. S8G shows that ectopic expression of all eight TSGs tested markedly suppressed tumor growth.

Next we asked whether knockdown of TSGs that encode repressors of FGFR signaling would transform SA cells. We first tested whether increased FGFR signaling was sufficient for transformation of these cells. SA cells ectopically expressing FGFR1, but not empty vector, formed colonies in soft agar (Fig. 4A) and tumors following subcutaneous injection into nude mice (Fig. 4B). Knockdown of all 17 TSGs that encode repressors of FGFR signaling enabled SA cells to form colonies in soft agar (Fig. 4C). Following knockdown, 14 of these 17 TSGs increased colony formation >5-fold and were further analyzed in a tumorigenicity assay. Notably, all 14 SA knockdown cell lines formed tumors following

subcutaneous injection into nude mice (Fig. 4D). As expected, pFRS2-Y436 levels were higher in all 14 tumors compared to those formed from *HRAS*-transformed SA cells, indicative of increased FGFR signaling (Supplementary Fig. S9A). Comparable results were obtained with a second, unrelated shRNA targeting each TSG (Supplementary Fig. S9B–D).

Knockdown of FGFR Signaling Repressors Sensitizes HBECs to FGFR Pharmacological Inhibition

Human cancer cell lines in which *FGFR1* is amplified or contains an activating mutation are sensitive to FGFR pharmacological inhibitors (27). We therefore hypothesized that knockdown of TSGs that encode repressors of FGFR signaling would sensitize cells to FGFR inhibitors. In these experiments we used ponatinib, a multi-targeted tyrosine kinase inhibitor that displays potent pan-FGFR inhibition at nanomolar concentrations (27). As controls, we used *HRAS*-transformed SA cells, whose ponatinib sensitivity is similar to that of parental SA cells (Supplementary Fig. S10A), as well as NCI-H520 cells, which are highly sensitive to FGFR inhibitors. In these experiments, we analyzed the 24 TSGs that were down-regulated in hLSCCs, 17 of which repress FGFR signaling and the other seven provided important negative controls.

The ponatinib titration experiment of Fig. 5A and B shows that SA knockdown cell lines that have increased tFGFR1 or pFGFR1 were highly sensitive to ponatinib treatment (see also Supplementary Fig. S10B and S10C). In fact, the ponatinib sensitivity of several of these SA knockdown cell lines was comparable to that of NCI-H520 cells. By contrast, most SA cell lines depleted of TSGs that encode FGFR1-independent FRS2 activators, or that do not affect FGFR signaling, were, by comparison, relatively ponatinib insensitive. As expected, SA cells in which *FGFR1* was ectopically over-expressed were also ponatinib sensitive (Supplementary Fig. S10D).

Ponatinib can inhibit multiple tyrosine kinases in addition to FGFR1 (see, for example, (27)). As an additional control for specificity, we analyzed the effect of shRNA-mediated depletion of FRS2, a downstream effector of all FGFRs, in the SA knockdown cell lines. Figure 5C shows that SA knockdown cell lines with increased tFGFR1 or pFGFR1 were sensitive to FRS2 depletion (see also Supplementary Fig. S10E). This result strongly suggests that the ponatinib sensitivity in these SA knockdown cell lines was, as expected, due to inhibition of FGFR signaling. Notably, SA cell lines depleted of TSGs that encode FGFR1-independent FRS2 activators were also sensitive to FRS2 depletion. Finally, the majority of SA cell lines depleted of TSGs that do not affect FRGR signaling were, as expected, relatively insensitive to FRS2 depletion.

These findings raise the possibility that some hLSCCs without *FGFR1* amplification or activating mutations may be sensitive to FGFR inhibitors. To test this possibility we analyzed A427 cells, a human lung carcinoma cell line that lacks *FGFR1* amplification or activating mutations but is unexpectedly sensitive to FGFR inhibitors (20). We first analyzed expression of the 24 TSGs that were down-regulated in hLSCCs (see Fig. 2) and found that three—*DAPP1*, *MYD88* and *STK11*—were substantially down-regulated in A427 cells compared to SA cells (Fig. 5D) or an independent immortalized but not transformed HBEC cell line (Supplementary Fig. S11). We then knocked down these three TSGs in SA

cells, both singly and in combination, and measured ponatinib sensitivity in a soft agar colony formation assay. The results of Fig. 5E show that TSG knockdown resulted in increased ponatinib sensitivity and this effect was greater with multiple compared to single knockdowns. Notably, the ponatinib sensitivity of SA cells depleted of all three TSGs was comparable to that of A427 cells. TSG knockdown also increased the proliferation rate of SA cells and again this effect was greater with multiple compared to single knockdowns (Supplementary Fig. S12).

The Splicing Regulator SRSF9 Represses FGFR Signaling Through the Cytoplasmic Adaptor Protein SH3BP2

One of the TSGs, *SRSF9*, encodes a member of a family of RNA-binding proteins that regulate pre-mRNA splicing (28). We were intrigued by how a splicing factor could modulate tFGFR1 levels (see Fig. 3) and hypothesized that SRSF9 might regulate splicing of a pre-mRNA encoding a protein involved in FGFR1 expression or stability. We therefore performed transcriptome profiling (RNA-Seq) experiments to identify pre-mRNAs whose splicing is altered by loss of SRSF9. Briefly, total RNA was isolated from SA cells stably expressing an SRSF9 shRNA or non-silencing control, and RNA samples were processed and amplified followed by paired-end deep sequencing (Fig. 6A). Using stringent selection criteria (see Methods), we identified 10 pre-mRNAs whose splicing was significantly altered in SRSF9 knockdown cells, several of which, including *EIF3C* (29, 30), *BCL2L11* (31) and *APC* (32), encode proteins that have been implicated in transformation-related activities (Supplementary Table S4). However, we thought the most potentially relevant to FGFR signaling was *SH3BP2* pre-mRNA, which encodes a cytoplasmic adaptor protein previously reported to interact with several tyrosine kinases including FGFR1 (33).

The RNA-Seq analysis indicated that knockdown of SRSF9 led to exclusion of *SH3BP2* exon 10. To validate the RNA-Seq results, we analyzed *SH3BP2* pre-mRNA splicing in two independent SRSF9 knockdown SA cell lines derived using unrelated SRSF9 shRNAs. Consistent with the RNA-Seq data, the qRT-PCR results of Fig. 6B show that following SRSF9 knockdown the level of *SH3BP2* exon 10 was substantially reduced, whereas total *SH3BP2* mRNA levels, monitored by analysis of unaffected exons 7 and 8, were normal. Exon 10 exclusion results in a frameshift that creates a premature stop codon (Fig. 6C). Accordingly, the immunoblot results of Fig. 6D show that full-length SH3BP2 protein levels were reduced in SRSF9 knockdown SA cells. Notably, the expected truncated SH3BP2 isoform was not detected, suggesting it was unstable. Consistent with this idea, in an ectopic expression experiment, full-length SH3BP2 could be readily detected whereas an engineered truncated SH3BP2 protein was again undetectable (Supplementary Fig. S13A–B).

We next determined how a reduction in SH3BP2 levels affected FGFR1. Figure 6E shows that shRNA-mediated knockdown of SH3BP2 resulted in increased levels of both pFGFR1 and tFGFR1. Conversely, ectopic expression of SH3BP2 led to reduced tFGFR1 levels (Fig. 6F). Finally, the co-immunoprecipitation experiment of Fig. 6G shows, consistent with the previous report (33), that SH3BP2 and FGFR1 are physically associated in SA cells.

Notably, similar to SRSF9 knockdown, knockdown of SH3BP2 promoted colony formation in soft agar (Fig. 6H) and tumor formation in mice (Fig. 6I), strongly suggesting that

SH3BP2 is the key target through which SRSF9 suppresses tumorigenesis. Collectively, these results suggest a model (Fig. 6J) in which SH3BP2 interacts with FGFR1, resulting in decreased FGFR1 levels. Loss of SRSF9 alters *SH3BP2* pre-mRNA splicing, leading to decreased levels of SH3BP2 and a corresponding increase in FGFR1 levels, resulting in increased FGFR signaling and transformation. Consistent with this idea, knockdown of FRS2 or treatment with ponatinib significantly suppressed growth of tumors derived from SRSF9 knockdown SA cells (Supplementary Fig. S14A–C), indicating that tumor growth is dependent upon FGFR signaling. Although it is possible that mis-splicing of pre-mRNAs other than *SH3BP2* may contribute to activation of FGFR signaling and transformation, our results indicate that mis-splicing of *SH3BP2* pre-mRNA is sufficient to promote both of these activities.

Finally, to determine the clinical relevance of these results, we analyzed the *SH3BP2* splicing pattern in hLSCC patient samples. The results of Fig. 6K show that in hLSCC samples in which *SRSF9* was markedly down-regulated (see Fig. 2A) there was also substantial *SH3BP2* exon 10 exclusion. By contrast, the extent of *SH3BP2* exon 10 exclusion was significantly less in lung adenocarcinoma samples in which *SRSF9* was only modestly down-regulated (see Fig. 2B). Collectively, these results reveal a strong correlation between *SRSF9* down-regulation and *SH3BP2* exon 10 exclusion in human lung cancers.

DISCUSSION

An RNAi-Based Mouse Tumorigenesis Screen for Identifying TSGs

Here we have described an experimental strategy for the systematic identification of candidate TSGs. Analysis of the original 28 human TSG candidates using the NCBI SKY/M-FISH and CGH database (National Center for Biotechnology Information Spectral Karyotyping, Multiplex Fluorescence In Situ Hybridization and Comparative Genomic Hybridization; (34)) revealed that all the genes have been found to harbor deletions in either one or both copies in multiple cancer types (Supplementary Table S5). Similarly, analysis of the COSMIC (Catalogue of Somatic Mutations in Cancer) database (35) revealed that all of the TSG candidates have been found to have loss of heterozygosity in one or more cancer types, six have been found to harbor homozygous deletions, and 11 have been found to be recurrently mutated in various cancers (Supplementary Table S6). In addition, a query of The Cancer Genome Atlas Lung Squamous Cell Carcinoma project database (36) revealed that eight of the TSGs have high frequency promoter hypermethylation in hLSCC samples (Supplementary Table S7). These findings provide additional support for the role of these genes as clinically relevant tumor suppressors.

Several of the genes we identified were previously unrecognized TSGs, with well-established roles in processes other than growth suppression. For example, *MYD88* is a gene best known for its role in innate immunity (reviewed in (37)) and, as described above, *SRSF9* encodes a pre-mRNA splicing factor (28). Our results highlight the power of unbiased, large-scale functional screening for cancer gene discovery.

Our screening strategy did not emphasize reaching saturation but rather sought to follow-up by directed experiments candidate TSGs isolated in the primary screen. Our reconstruction

experiment indicates that, in principle, the design of the primary screen was sufficient to analyze all 62,400 shRNAs in the library. However, we suspect that our screen, like other large-scale shRNA screens (see, for example, (38)), did not achieve saturation for reasons including suboptimal efficacy of some shRNAs (39), unequal representation of shRNAs in the primary screen, and an insufficient depth of sequencing.

In addition, intrinsic limitations of the cell line used in the primary screen prevented identification of all TSGs. For example, in NIH 3T3 cells the TP53 pathway is inactivated due to biallelic deletion of the *INK4A*/*ARF* (*CDKN2A*/*CDKN2B*) locus. Thus, although *TP53* and *CDKN2A* are TSGs that are frequently inactivated in a variety of cancers including hLSCC (35), they would not have been isolated in our screen.

New hLSCC Tumor Suppressors that Repress FGFR Signaling

Following the identification of candidate TSGs from the primary screen, we then carried out a series of bioinformatic, comparative expression and functional experiments in human lung cancer samples and cell lines, which revealed that many of the genes identified in the primary screen were hLSCC TSGs. We speculate that NIH 3T3 cells are particularly effective in identifying hLSCC TSGs because they are a fibroblast cell line and, as discussed above, FGFR signaling plays an important role in hLSCC development. Consistent with this idea, both NIH 3T3 cells and HBECs are transformed by ectopic expression of FGFR1 or knockdown of FGFR signaling repressors (Figs. 1C, 3A and 4A–D).

Unexpectedly, we found that 17 of the 24 hLSCC TSGs encode repressors of FGFR signaling. For several of the TSGs, the mechanism by which FGFR signaling is repressed can be readily envisioned. For example, PTPN4, which we found inhibits FGFR1 phosphorylation, is a known tyrosine phosphatase (40), suggesting that FGFR1 is a substrate of PTPN4. GAPVD1 has been shown to mediate ubiquitination and degradation of EGFR (41) and may similarly regulate tFGFR1. However, for most TSGs the basis by which FGFR signaling is repressed remains to be determined, and could occur through either direct or indirect mechanisms.

Several considerations allow us to conclude that the basis of transformation of HBECs following knockdown of the 17 TSGs that encode repressors of FGFR signaling is, in fact, increased FGFR signaling. First, ectopic expression of FGFR1 is sufficient to transform HBECs (Fig. 4D). Second, following knockdown of the TSG, FGFR signaling is increased (Fig. 3B). Third, the transformed HBEC lines are sensitized to inhibition of FGFR signaling either by ponatinib addition (Fig. 5A and B) or FRS2 knockdown (Fig. 5C).

An important implication of our results is that aberrantly increased FGFR signaling may drive tumorigenesis of many hLSCCs that lack FGFR1 amplification or activating mutations. Moreover, the increased FGFR signaling could render these hLSCCs sensitive to FGFR pharmacological inhibitors as we found in our cell culture experiments. Consistent with these ideas, a recent study analyzed a large collection of more than 500 human cancer cell lines for sensitivity to the FGFR inhibitor NVP-BGJ398, and found that 37.5% of the drug-sensitive cell lines lacked genetic abnormalities in FGF and FGFRs (42). We note, however, that to date FGFR inhibitors have not been proven to be clinically effective, which

may be due to several factors including improper patient selection, use of non-optimized drugs, and not using appropriate drug combinations (43).

Functional Genomic Approaches for Identification of Epigenetically Silenced TSGs

Functional genomics approaches for TSG discovery are highly complementary to cancer genome sequencing efforts. For example, a recent hLSCC genomic sequencing study (13) reported statistically recurrent mutations in 11 genes but only one of these, *STK11*, was in common with the 24 TSGs identified in this study. Thus, we discovered many hLSCC TSGs that were not identified by cancer genome sequencing, apparently because they are inactivated by transcriptional repression and not mutation.

METHODS

Cell Lines and Culture

NIH 3T3, *KRas* NIH 3T3, NCI-H520 and A427 cells were obtained from the American Type Culture Collection (ATCC) and grown as recommended by the supplier. SA cells (provided by S. Randell) and HBECs (provided by J. Minna) were grown in BEGM medium (Lonza). NIH 3T3 cells, *KRas* NIH 3T3 cells, SA cells and HBECs were routinely tested in soft agar colony formation and mouse xenograft assays to confirm the expected transformed or non-transformed phenotype. Otherwise, the cell lines used were not authenticated.

RNA Interference Screening

For the reconstruction experiment, 0, 100 or 1000 *Kras*-transformed NIH 3T3 cells were mixed with NIH 3T3 cells to achieve a final population of 1×10^6 cells, and injected into the flanks of BALB/c nu/nu mice (n=3; Taconic Farms). Tumor dimensions were measured every 1–2 days, and tumor volume was calculated using the formula $\pi/4 \times (\text{length}) \times (\text{width})^2$.

Using the mouse shRNA^{mir} library (release 2.16; Open Biosystems/Thermo Scientific), 10 retroviral pools were generated as previously described (44). NIH 3T3 cells (1×10^6) were transduced at a multiplicity of infection (MOI) of 0.2 with the retroviral stocks, and 2 days later selected for resistance to puromycin (1.5 μg/ml) for 7 days. For each pool, 1×10^6 cells were injected subcutaneously into the flank of a nude mouse. Tumors were excised and dissected, genomic DNA was extracted, and shRNAs were identified as previously described (44).

To validate candidates, NIH 3T3 cells (1×10^6) were infected with a retrovirus carrying an individual shRNA (listed in Supplementary Table S8) and puromycin selected for 1 week. NIH 3T3 knockdown cells (2×10^6) were injected subcutaneously into nude mice (n=2); mice were sacrificed and photographed when the tumor size reached 1.5 cm. Animal protocols were approved by the Institution Animal Care and Use Committee at UMass Medical School.

For all 32 genes whose knockdown promoted tumor formation, a second, unrelated shRNA directed against the same target gene was tested for promotion of colony formation in soft

agar and knockdown efficiency of the target gene. Only candidates that validated with two shRNAs, both of which knocked down the target gene, were considered further.

Quantitative RT-PCR

Total RNA was isolated using TriPure Isolation Reagent (Roche). Reverse transcription was performed using SuperScript II Reverse Transcriptase (Invitrogen) followed by qPCR using Fast SYBR Green Master Mix (Applied Biosystems) using primers listed in Supplementary Table S9. The expression level of each gene was normalized to that of *GAPDH*.

Soft Agar Colony Formation Assays

NIH 3T3 knockdown cells (5×10^3) were seeded using a CytoSelect 96-Well Cell Transformation Assay Kit (Cell Biolabs). For quantification, colonies with >10 cells were counted and normalized to that obtained with a non-silencing shRNA, which was set to 1 (Supplementary Fig. S1B) or cells were lysed, stained with CyQuant and analyzed using a 1420 Victor Multilabel Counter (Perkin Elmer) and a 480/520 nm filter set (Supplementary Fig. S1C). Ponatinib (Selleck) was added to the medium at the concentration(s) indicated in Fig. 5A and B, and soft agar colony formation assays were performed.

Identification of Human Homologs

Human genes, identified using NCBI's HomoloGene, were considered to be homologs if they shared greater than 50% identity at the protein level with the mouse gene.

Expression Analysis in Human Lung Cancer Samples

Total RNA from nine normal lung, 10 lung adenocarcinoma and 27 hLSCC samples were obtained from the UMMS Cancer Center Tissue Bank. qRT-PCR was performed using primers listed in Supplementary Table S9. Boxplots and statistical analyses were done using R (45). Wilcoxon rank sum test was performed to determine whether expression of each TSG or SH3BP2 exon 10 in hLSCC or human lung adenocarcinoma samples significantly differed from that in normal lung. In Fig. 2, to correct for multiple comparisons, *P*-values were adjusted using Bonferroni method and genes with an adjusted *P*-value <0.05 were considered significant. A gene was considered "positive" if it was down-regulated >2-fold in ≥70% of the samples and had a *P*-value <0.05. In Fig. 6K, the results were normalized to that obtained in SA cells to correct for differences in primer efficiencies.

Immunoblot Analysis

Immunoblots were probed using antibodies against tEGFR (Cell Signaling), pERK1/2, tERK1/2 (Cell Signaling Technology), pFGFR1, tFGFR1 (Invitrogen), tFGFR2, tFGFR3 () and tFGFR4 (Santa Cruz). pFRS2-Y436 (Abcam), pFRS2-Y196 (Cell Signaling), tFRS2 (Santa Cruz), tIR (Cell Signaling), tPLC γ (Santa Cruz), SH3BP2 (Abcam), pY (Invitrogen), and α-tubulin. Pairwise p- and t- proteins were analyzed on separate gels/immunoblots using the same protein lysate. Immunoblots were quantified using Image J software (NIH). For the co-immunoprecipitation experiments of Fig. 6G, the FGFR1 or SH3BP2 antibody was conjugated to Dynabeads (Invitrogen) overnight, added to NCI-H520 cell extract and incubated at 4°C overnight.

Ectopic FGFR1 Expression

The human or mouse *FGFR1* cDNA clone (MHS1010-7429513 or MMM1013-7510432, respectively; Open Biosystems/Thermo Scientific) and empty vector (pCMV-SPORT6; Open Biosystems) were transfected into SA or NIH 3T3 cells twice with 3 days in between to achieve maximum transfection efficiency. For soft agar colony formation assays, 1×10^4 cells were plated and colony number was counted after 3 weeks. For tumor formation assays, 2×10^6 NIH 3T3 or 1×10^7 SA cells expressing FGFR1 or vector were injected into nude mice (n=3).

Ectopic Expression of TSGs

TSG cDNAs (see Supplementary Table S10) were cloned, by PCR (using primers listed in Supplementary Table S9) followed by restriction enzyme digestion, into MSCV PIG (Puro-IRES-GFP) (Addgene plasmid 18751). For some genes, a 3xFlag tag sequence was incorporated into the primers for cloning in-frame with the target gene. For further details, please refer to the Supplementary Methods.

Analysis of SA Knockdown Cells for Transformation Activity

To generate SA knockdown cell lines, SA cells (5×10^3) were plated in 6-well plates and infected with a lentivirus expressing an individual shRNA at an MOI of 2. Soft agar colony formation and tumor formation assays were performed as described above. For Fig. 5C, TSG knockdown SA cells were plated in 96-well plates and infected with an FRS2 or non-silencing shRNA. Cell viability was monitored using PrestoBlue (Invitrogen).

RNA-Seq

Total RNA from non-silencing or SRSF9 knockdown SA cells was isolated using TriPure Isolation Reagent (Roche), and mRNA purification, cDNA synthesis and amplification were carried out according to the TrueSeq RNA sample preparation guide (Illumina). Libraries were sequenced as 100-bp paired end using Illumina HiSeq 2000. All reads were mapped to the human genome (hg19) using TopHat, followed by running Cufflinks to assemble and quantify the transcriptome (46). Alternative splicing events were first determined using Cuffdiff2 and further analyzed as follows. Gene-level normalized isoform expression (NI) is defined as the ratio of the isoform level to the gene level (isoform FPKM/gene FPKM). Relative difference of NI (RDni), a differential alternative splicing event measurement, was calculated as (NI for knockdown/NI for non-silencing). Absolute difference of NI (ADni) was calculated as |NI for knockdown - NI for non-silencing | to indicate the magnitude of the alternative splicing. Isoforms with RDni >1.2 or <1/1.2, and ADni >0.1, and gene level expression greater than median FPKM in both conditions (Supplementary Table S4) were selected for further validation. The RNA-Seq data have been deposited in NCBI's Gene Expression Omnibus (47) and are accessible through GEO Series accession number GSE47095.

Ectopic SH3BP2 Expression

The full length *SH3BP2* cDNA clone was obtained from the MGC collection (catalog #5103986). The truncated protein was generated using the QuikChange Lightning Site-

Directed Mutagenesis Kit (Agilent) with primers For 5′-GACGAGGACTATGAGAAGGTTGTTCAAGGCTACAAG-3′ and Rev 5′-CTTGTAGCCTTGAACAACCTTCTCATAGTCCTCGTC-3′.

Database Mining

The Oncomine 4.3 Cancer Profiling Database was searched using a threshold p-value of 0.05, fold change of 2 and gene rank of “All”. The NCI/NCBI SKY/M-FISH & CGH Database was queried using NCBI’s Entrez system Cancer Chromosomes, using the human chromosome location based on cytogenetic band information according to Entrez Gene. Searches of the COSMIC database were performed using release v63. Searches of the lung squamous cell carcinoma dataset using The Cancer Genome Atlas Data Portal queried DNA promoter methylation frequency using a criterion of ≥0.5 (intensity ratio of methylated and unmethylated DNA).

Statistical Analysis

All quantitative data were collected from experiments performed in at least triplicate, and expressed as mean ± SD. Differences between groups were assayed by two-tailed student *t*-test in Microsoft Excel using unpaired (Fig. 5B, 5C, 5D, 6B) or paired (Fig. 4C, 6H) comparisons. Significant differences were considered when $P \leq 0.05$; $*P < 0.05$ and $**P < 0.01$.

Supplementary Material

Refer to Web version on PubMed Central for supplementary material.

Acknowledgments

We thank S. Lowe, S. Randell, J. Minna and R. Tikkanen for providing reagents; The University of Massachusetts RNAi Core for providing shRNA clones and pools and cDNA clones; L. Girard, J. Heymach and J. D. Minna for helpful discussions and sharing unpublished results; S. Griggs for assistance with the animal experiments; and S. Deibler for editorial assistance.

Grant Support

This work was supported in part by NIH grant R01GM035490 to M.R. Green. M.R. Green is an investigator of the Howard Hughes Medical Institute.

Abbreviations list

COSMIC	Catalogue of Somatic Mutations in Cancer
EGFR	epidermal growth factor receptor
FGFR1	fibroblast growth factor receptor 1
GFP	green fluorescence protein
HBECs	human bronchial epithelial cells
hLSCCs	human lung squamous cell carcinomas
IR	insulin receptor

MAPK	mitogen-activated protein kinase
NCBI SKY/M-FISH and CGH	National Center for Biotechnology Information Spectral Karyotyping, Multiplex Fluorescence In Situ Hybridization and Comparative Genomic Hybridization
pERK1/2	phosphorylated ERK1/2
pFGFR1	phosphorylated FGFR1
pFRS2-Y436	phosphorylated FRS2-Y436
PLC-γ	phospholipase C-γ
qRT-PCR	quantitative real-time RT-PCR
RNAi	RNA interference
shRNA	short hairpin RNA
tFGFR1	total FGFR1
tFRS2	total FRS2
TSGs	tumor suppressor genes

References

1. Mardis ER, Wilson RK. Cancer genome sequencing: a review. Hum Mol Genet. 2009; 18:R163–8. [PubMed: 19808792]
2. Loeb LA. A mutator phenotype in cancer. Cancer Res. 2001; 61:3230–9. [PubMed: 11309271]
3. Esteller M. Epigenetic gene silencing in cancer: the DNA hypermethylome. Hum Mol Genet. 2007; 16(Spec No 1):R50–9. [PubMed: 17613547]
4. Stacey DW, Kung HF. Transformation of NIH 3T3 cells by microinjection of Ha-ras p21 protein. Nature. 1984; 310:508–11. [PubMed: 6611509]
5. Smith MR, Heidecker G, Rapp UR, Kung HF. Induction of transformation and DNA synthesis after microinjection of raf proteins. Mol Cell Biol. 1990; 10:3828–33. [PubMed: 2192265]
6. Velu TJ, Beguinot L, Vass WC, Willingham MC, Merlino GT, Pastan I, et al. Epidermal-growth-factor-dependent transformation by a human EGF receptor proto-oncogene. Science. 1987; 238:1408–10. [PubMed: 3500513]
7. Di Fiore PP, Pierce JH, Kraus MH, Segatto O, King CR, Aaronson SA. erbB-2 is a potent oncogene when overexpressed in NIH/3T3 cells. Science. 1987; 237:178–82. [PubMed: 2885917]
8. Silva JM, Li MZ, Chang K, Ge W, Golding MC, Rickles RJ, et al. Second-generation shRNA libraries covering the mouse and human genomes. Nat Genet. 2005; 37:1281–8. [PubMed: 16200065]
9. Harris LK, Westwood M. Biology and significance of signalling pathways activated by IGF-II. Growth Factors. 2012; 30:1–12. [PubMed: 22136428]
10. Gaur P, Bielenberg DR, Samuel S, Bose D, Zhou Y, Gray MJ, et al. Role of class 3 semaphorins and their receptors in tumor growth and angiogenesis. Clin Cancer Res. 2009; 15:6763–70. [PubMed: 19887479]
11. Korsse SE, Peppelenbosch MP, van Veelen W. Targeting LKB1 signaling in cancer. Biochim Biophys Acta. 2013; 1835:194–210. [PubMed: 23287572]
12. Rhodes DR, Kalyana-Sundaram S, Tomlins SA, Mahavisno V, Kasper N, Varambally R, et al. Molecular concepts analysis links tumors, pathways, mechanisms, and drugs. Neoplasia. 2007; 9:443–54. [PubMed: 17534450]

13. Hammerman PS, Hayes DN, Wilkerson MD, Schultz N, Bose R, Chu A, et al. Comprehensive genomic characterization of squamous cell lung cancers. Nature. 2012; 489:519–25. [PubMed: 22960745]
14. Bibikova M, Le J, Barnes B, Saedinia-Melnyk S, Zhou L, Shen R, et al. Genome-wide DNA methylation profiling using Infinium assay. Epigenomics. 2009; 1:177–200. [PubMed: 22122642]
15. Stearman RS, Grady MC, Nana-Sinkam P, Varella-Garcia M, Geraci MW. Genetic and epigenetic regulation of the human prostacyclin synthase promoter in lung cancer cell lines. Mol Cancer Res. 2007; 5:295–308. [PubMed: 17374734]
16. Gray SG, Al-Sarraf N, Baird AM, Cathcart MC, McGovern E, O'Byrne KJ. Regulation of EP receptors in non-small cell lung cancer by epigenetic modifications. Eur J Cancer. 2009; 45:3087–97. [PubMed: 19818596]
17. Ito M, Ito G, Kondo M, Uchiyama M, Fukui T, Mori S, et al. Frequent inactivation of RASSF1A, BLU, and SEMA3B on 3p21. 3 by promoter hypermethylation and allele loss in non-small cell lung cancer. Cancer Lett. 2005; 225:131–9. [PubMed: 15922865]
18. Kuroki T, Trapasso F, Yendamuri S, Matsuyama A, Alder H, Williams NN, et al. Allelic loss on chromosome 3p21. 3 and promoter hypermethylation of semaphorin 3B in non-small cell lung cancer. Cancer Res. 2003; 63:3352–5. [PubMed: 12810670]
19. Dutt A, Ramos AH, Hammerman PS, Mermel C, Cho J, Sharifnia T, et al. Inhibitor-sensitive FGFR1 amplification in human non-small cell lung cancer. PLoS One. 2011; 6:e20351. [PubMed: 21666749]
20. Weiss J, Sos ML, Seidel D, Peifer M, Zander T, Heuckmann JM, et al. Frequent and focal FGFR1 amplification associates with therapeutically tractable FGFR1 dependency in squamous cell lung cancer. Sci Transl Med. 2010; 2:62ra93.
21. Kouhara H, Kurebayashi S, Hashimoto K, Kasayama S, Koga M, Kishimoto T, et al. Ligand-independent activation of tyrosine kinase in fibroblast growth factor receptor 1 by fusion with beta-galactosidase. Oncogene. 1995; 10:2315–22. [PubMed: 7784079]
22. Lundberg AS, Randell SH, Stewart SA, Elenbaas B, Hartwell KA, Brooks MW, et al. Immortalization and transformation of primary human airway epithelial cells by gene transfer. Oncogene. 2002; 21:4577–86. [PubMed: 12085236]
23. Eswarakumar VP, Lax I, Schlessinger J. Cellular signaling by fibroblast growth factor receptors. Cytokine Growth Factor Rev. 2005; 16:139–49. [PubMed: 15863030]
24. El-Shewy HM, Lee MH, Obeid LM, Jaffa AA, Luttrell LM. The insulin-like growth factor type 1 and insulin-like growth factor type 2/mannose-6-phosphate receptors independently regulate ERK1/2 activity in HEK293 cells. J Biol Chem. 2007; 282:26150–7. [PubMed: 17620336]
25. McKinnon T, Chakraborty C, Gleeson LM, Chidiac P, Lala PK. Stimulation of human extravillous trophoblast migration by IGF-II is mediated by IGF type 2 receptor involving inhibitory G protein(s) and phosphorylation of MAPK. J Clin Endocrinol Metab. 2001; 86:3665–74. [PubMed: 11502794]
26. Clarhaut J, Roche J, Drabkin HA. Semaphorins in lung cancer. J Thorac Oncol. 2006; 1:203–4. [PubMed: 17409857]
27. Gozgit JM, Wong MJ, Moran L, Wardwell S, Mohemmad QK, Narasimhan NI, et al. Ponatinib (AP24534), a multitargeted pan-FGFR inhibitor with activity in multiple FGFR-amplified or mutated cancer models. Mol Cancer Ther. 2012; 11:690–9. [PubMed: 22238366]
28. Screaton GR, Caceres JF, Mayeda A, Bell MV, Plebanski M, Jackson DG, et al. Identification and characterization of three members of the human SR family of pre-mRNA splicing factors. Embo J. 1995; 14:4336–49. [PubMed: 7556075]
29. Menon R, Omenn GS. Proteomic characterization of novel alternative splice variant proteins in human epidermal growth factor receptor 2/neu-induced breast cancers. Cancer Res. 2010; 70:3440–9. [PubMed: 20388783]
30. Zhang L, Pan X, Hershey JW. Individual overexpression of five subunits of human translation initiation factor eIF3 promotes malignant transformation of immortal fibroblast cells. J Biol Chem. 2007; 282:5790–800. [PubMed: 17170115]
31. Zhang J, Manley JL. Misregulation of pre-mRNA alternative splicing in cancer. Cancer Discov. 2013; 3:1228–37. [PubMed: 24145039]

32. Kalnina Z, Zayakin P, Silina K, Line A. Alterations of pre-mRNA splicing in cancer. Genes Chromosomes Cancer. 2005; 42:342–57. [PubMed: 15648050]
33. Hu Y, Fang X, Dunham SM, Prada C, Stachowiak EK, Stachowiak MK. 90-kDa ribosomal S6 kinase is a direct target for the nuclear fibroblast growth factor receptor 1 (FGFR1): role in FGFR1 signaling. J Biol Chem. 2004; 279:29325–35. [PubMed: 15117958]
34. Knutsen T, Gobu V, Knaus R, Padilla-Nash H, Augustus M, Strausberg RL, et al. The interactive online SKY/M-FISH & CGH database and the Entrez cancer chromosomes search database: linkage of chromosomal aberrations with the genome sequence. Genes Chromosomes Cancer. 2005; 44:52–64. [PubMed: 15934046]
35. Forbes SA, Bindal N, Bamford S, Cole C, Kok CY, Beare D, et al. COSMIC: mining complete cancer genomes in the Catalogue of Somatic Mutations in Cancer. Nucleic Acids Res. 2011; 39:D945–50. [PubMed: 20952405]
36. Network CGAR. Comprehensive genomic characterization of squamous cell lung cancers. Nature. 2012; 489:519–25. [PubMed: 22960745]
37. Arancibia SA, Beltran CJ, Aguirre IM, Silva P, Peralta AL, Malinarich F, et al. Toll-like receptors are key participants in innate immune responses. Biol Res. 2007; 40:97–112. [PubMed: 18064347]
38. Mullenders J, Bernards R. Loss-of-function genetic screens as a tool to improve the diagnosis and treatment of cancer. Oncogene. 2009; 28:4409–20. [PubMed: 19767776]
39. Bassik MC, Lebbink RJ, Churchman LS, Ingolia NT, Patena W, LeProust EM, et al. Rapid creation and quantitative monitoring of high coverage shRNA libraries. Nat Methods. 2009; 6:443–5. [PubMed: 19448642]
40. Park KW, Lee EJ, Lee S, Lee JE, Choi E, Kim BJ, et al. Molecular cloning and characterization of a protein tyrosine phosphatase enriched in testis, a putative murine homologue of human PTPMEG. Gene. 2000; 257:45–55. [PubMed: 11054567]
41. Su X, Kong C, Stahl PD. GAPex-5 mediates ubiquitination, trafficking, and degradation of epidermal growth factor receptor. J Biol Chem. 2007; 282:21278–84. [PubMed: 17545148]
42. Guagnano V, Kauffmann A, Wohrle S, Stamm C, Ito M, Barys L, et al. FGFR genetic alterations predict for sensitivity to NVP-BGJ398, a selective pan-FGFR inhibitor. Cancer Discov. 2012; 2:1118–33. [PubMed: 23002168]
43. Dieci MV, Arnedos M, Andre F, Soria JC. Fibroblast growth factor receptor inhibitors as a cancer treatment: from a biologic rationale to medical perspectives. Cancer Discov. 2013; 3:264–79. [PubMed: 23418312]
44. Gazin C, Wajapeyee N, Gobeil S, Virbasius CM, Green MR. An elaborate pathway required for Ras-mediated epigenetic silencing. Nature. 2007; 449:1073–7. [PubMed: 17960246]
45. Ihaka R, Gentleman R. R: A language for data analysis and graphics. J Comput Graph Stat. 1996; 5:299–314.
46. Trapnell C, Roberts A, Goff L, Pertea G, Kim D, Kelley DR, et al. Differential gene and transcript expression analysis of RNA-seq experiments with TopHat and Cufflinks. Nat Protoc. 2012; 7:562–78. [PubMed: 22383036]
47. Edgar R, Domrachev M, Lash AE. Gene Expression Omnibus: NCBI gene expression and hybridization array data repository. Nucleic Acids Res. 2002; 30:207–10. [PubMed: 11752295]

SIGNIFICANCE

A functional genomics approach identifies new lung tumor suppressor genes (TSGs) whose loss aberrantly increases FGFR signaling to promote tumorigenesis. These TSGs are frequently down-regulated in human lung squamous cell carcinomas (hLSCCs), indicating that increased FGFR signaling promotes tumorigenesis in many hLSCCs lacking FGFR1 amplification or activating mutations.

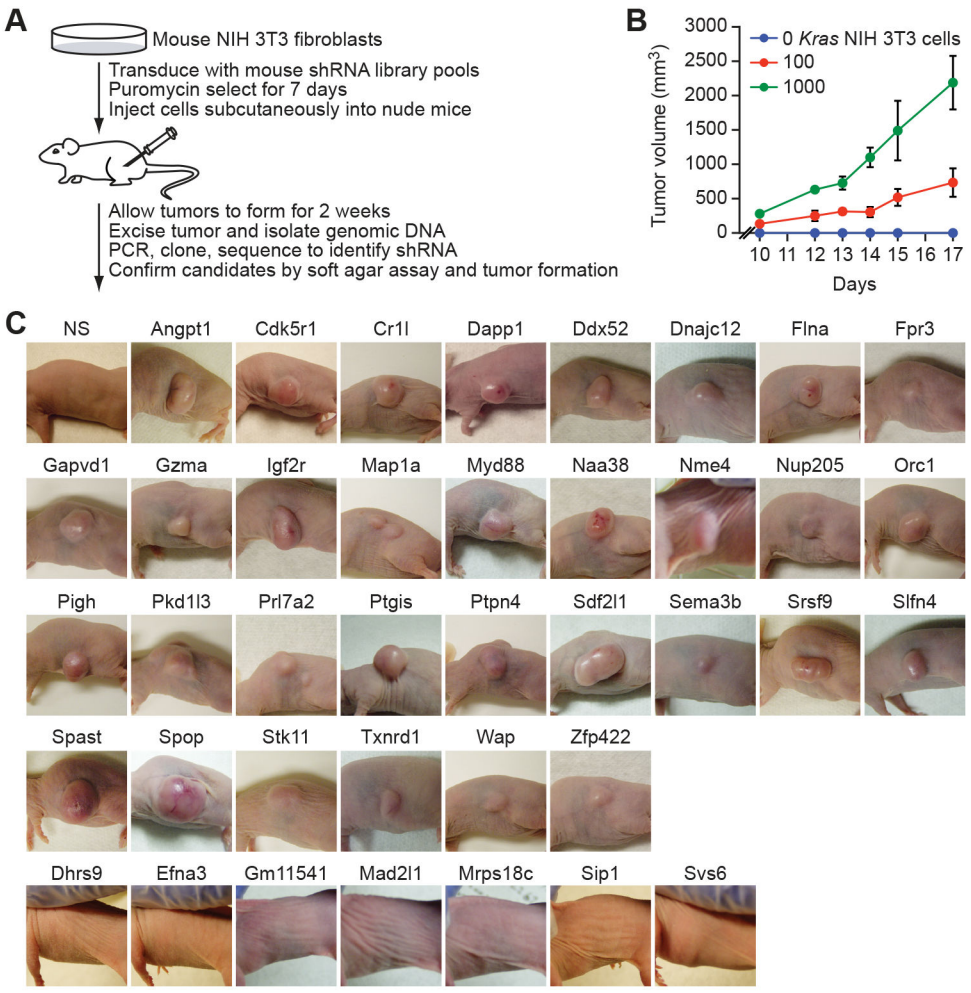

Figure 1.

A large-scale shRNA screen identifies candidate TSGs. **A**, Schematic summary of the screen. **B**, Tumor formation in mice (n=3) subcutaneously injected with 1×10^6 cells comprising a mixture of non-transformed NIH 3T3 cells and 0, 100 or 1000 *Kras*-transformed NIH 3T3 cells. Data are represented as mean ± SD. **C**, Tumor formation in mice injected with NIH 3T3 knockdown cell lines; tumors were photographed at various time points following injection. NS, non-silencing shRNA control.

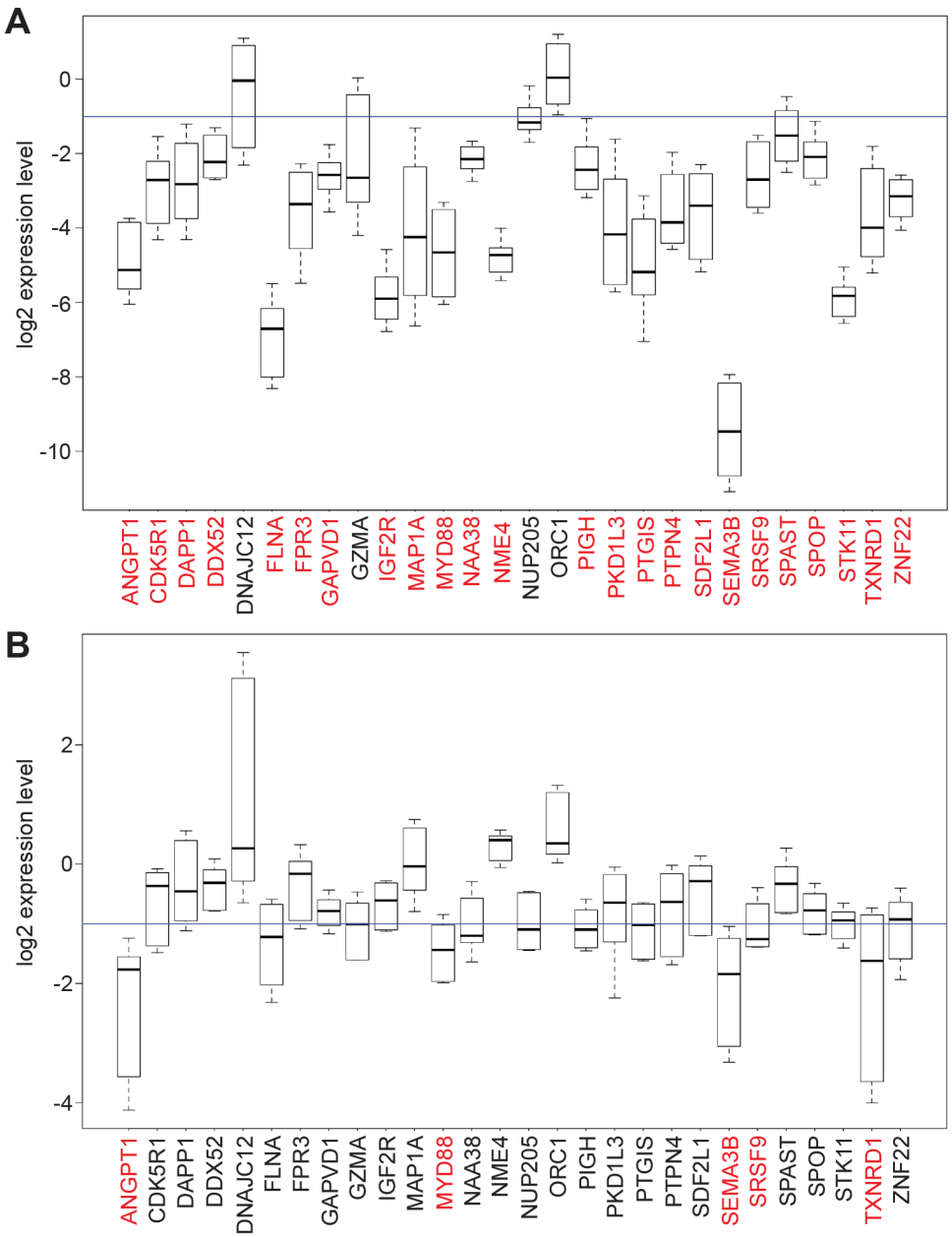

Figure 2.

Many candidate TSGs are down-regulated in hLSCC samples. **A** and **B**, Boxplots displaying log2 fold changes in expression of each TSG in 27 hLSCC samples (**A**) and 10 human lung adenocarcinoma samples (**B**) compared with the mean of nine normal lung samples. Boxed areas span the first to the third quartile. Whiskers represent 15th and 85th percentiles; samples falling outside these percentiles have been removed for clarity. The blue line indicates a 2-fold decrease in gene expression. Genes indicated in red are down-regulated >2-fold in ≥70% of the samples analyzed and have a *P*-value <0.05 (see Methods).

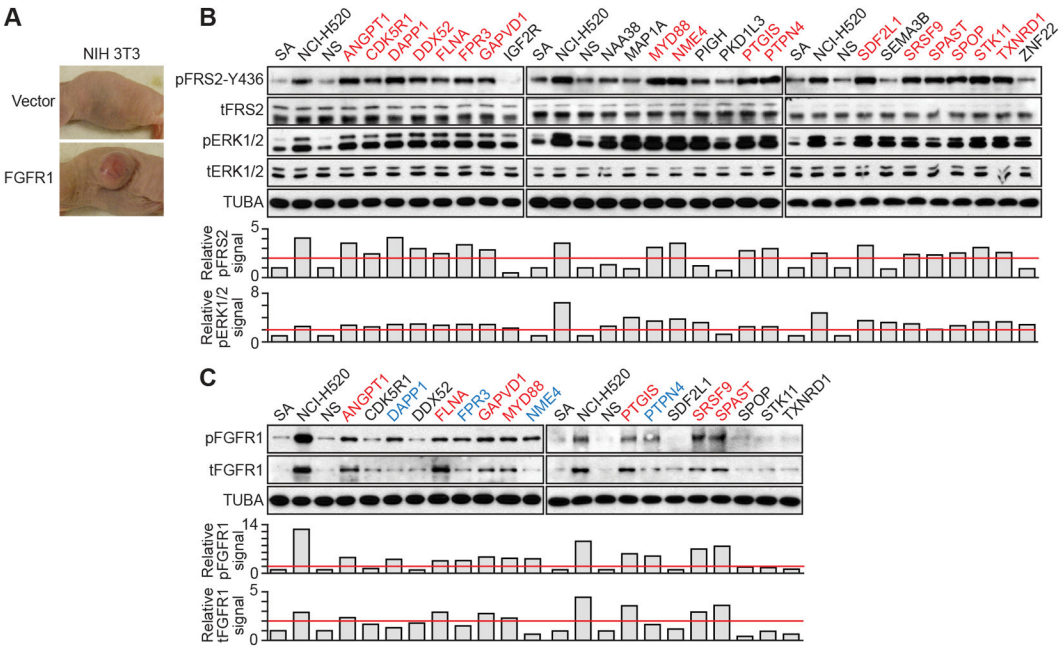

Figure 3.

Many of the TSGs encode repressors of FGFR signaling. **A**, Tumor formation 4 weeks following injection of NIH 3T3 cells expressing FGFR1 or, as a control, empty vector. **B** and **C**, (Top) Immunoblots monitoring phosphorylated (p) and total (t) FRS2 and ERK1/2 (**B**) or FGFR1 (**C**) in the SA knockdown cell lines and NCI-H520 cells. α-tubulin (TUBA) was monitored as a loading control. (Bottom) Quantification of the immunoblots. The red line indicates a two-fold increase in phospho-protein level relative to that observed in non-silencing (NS) cells, which was set to 1. Genes in red indicate those whose knockdown increases pFRS2-Y436 levels (**B**) or pFGFR1 and tFGFR1 levels (**C**); blue, increased pFGFR1 but not tFGFR1 levels; and black, no effect on either pFGFR1 or tFGFR1 levels.

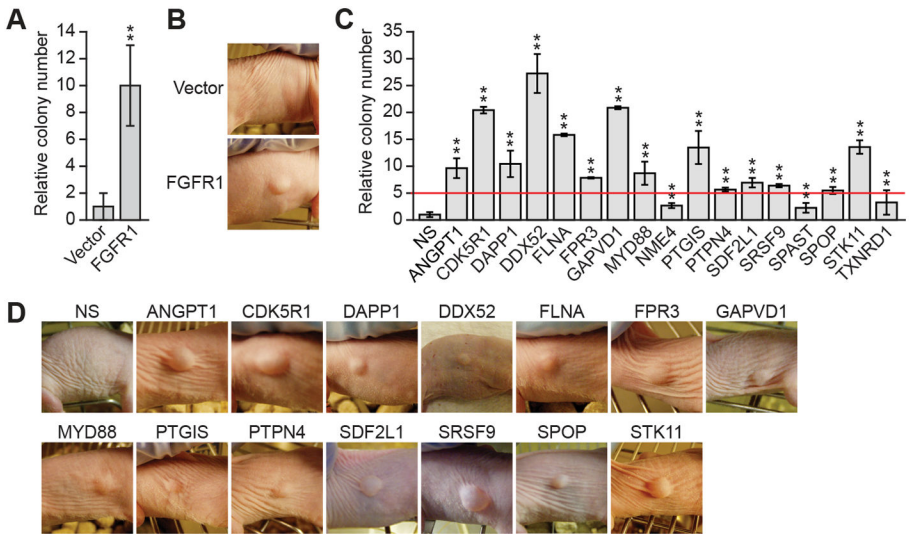

Figure 4.

Knockdown of FGFR signaling repressors transforms immortalized HBECs. **A**, Soft agar assay measuring colony formation of SA cells expressing FGFR1 relative to that obtained with empty vector, which was set to 1. Data are represented as mean ± SD. **B**, Tumor formation 6 weeks following injection of SA cells expressing FGFR1 or empty vector. **C**, Soft agar assay measuring colony formation of SA knockdown cell lines relative to that obtained with the non-silencing (NS) shRNA, which was set to 1. Data are represented as mean ± SD. **D**, Tumor formation in mice injected with SA knockdown cell lines; tumors were photographed at various time points following injection. **P*<0.05; ***P*<0.01.

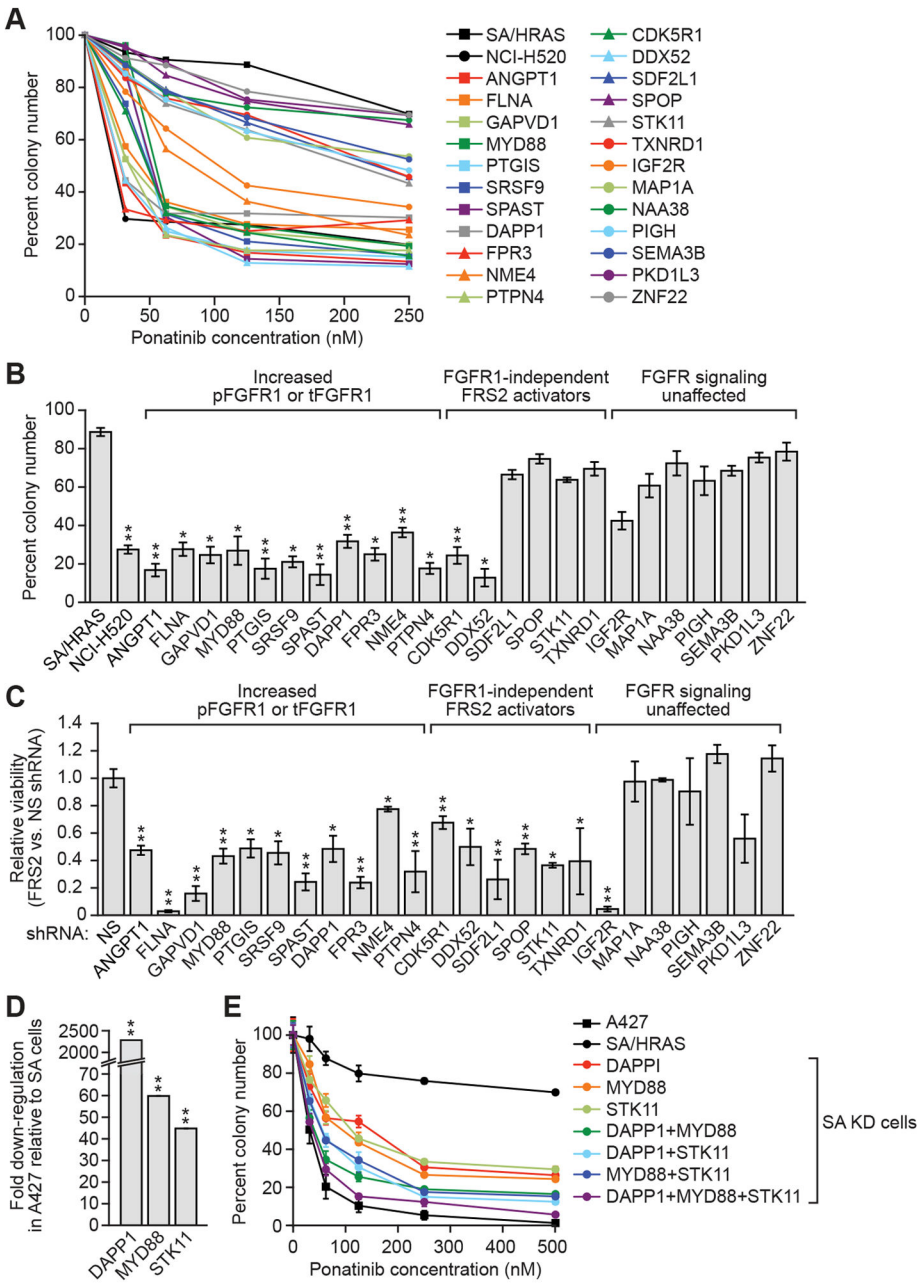

Figure 5.

Knockdown of FGFR signaling repressors sensitizes HBECs to FGFR pharmacological inhibition. **A**, Soft agar assay measuring colony formation of SA knockdown cells treated with varying concentrations of ponatinib. Colony number was normalized to that obtained in the absence of ponatinib, which was set to 100%. **B**, Soft agar assay measuring colony formation of SA knockdown cells treated with 125 nM ponatinib, normalized as described in (A). Data are represented as mean ± SD. **C**, Colony formation assay measuring viability of SA knockdown cells expressing an FRS2 shRNA relative to that obtained with a non-silencing (NS) shRNA. Viability was normalized to that obtained in NS shRNA-expressing

cells, which was set to 1. Data are represented as mean ± SD. **D**, qRT-PCR analysis monitoring expression of *DAPP1*, *MYD88* and *STK11* in A427 cells relative to SA cells. Data are represented as mean ± SD (error bars are too small to be visualized). **E**, Soft agar assay monitoring colony formation of ponatinib-treated SA single, double and triple knockdown (KD) cells, normalized as described in (A). Data are represented as mean ± SD. **P*<0.05; ***P*<0.01.

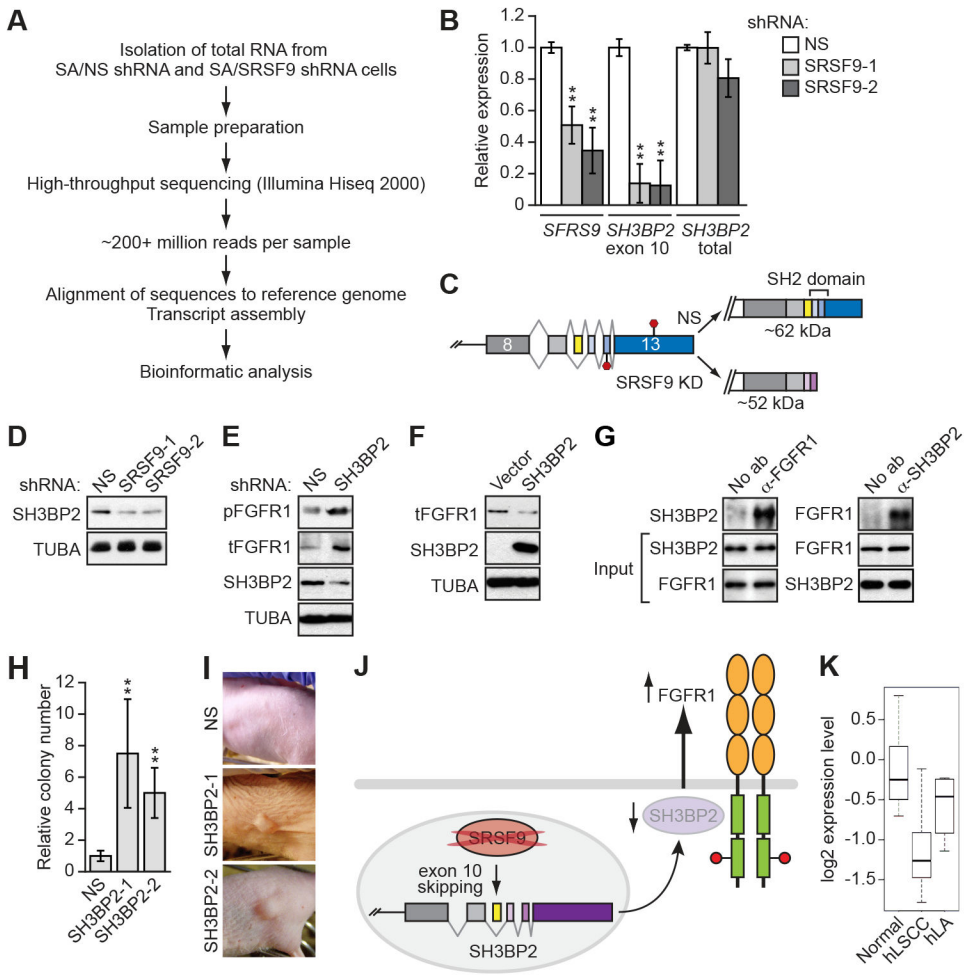

Figure 6.

The splicing regulator SRSF9 represses FGFR signaling through the cytoplasmic adaptor protein SH3BP2. **A**, Schematic of the RNA-Seq experimental approach and data analysis. **B**, qRT-PCR analysis monitoring expression of *SRSF9*, *SH3BP2* exon 10 and *SH3BP2* exons 7–8 (*SH3BP2* total) in SA cells expressing a non-silencing (NS) shRNA or one of two unrelated SRSF9 shRNAs. The results were normalized to expression in NS control cells, which was set to 1. **C**, Schematic showing splicing of the *SH3BP2* gene in NS and SRSF9 knockdown cells, in which exon 10 (yellow) is skipped. Red octagons indicate stop codons. The resulting proteins are also shown. In the truncated protein, the last two exons are shown in purple to indicate an alternate reading frame compared to the full-length protein. **D**, Immunoblot monitoring levels of SH3BP2 in SA cells expressing an NS or one of two SRSF9 shRNAs. **E and F**, Immunoblot analysis monitoring levels of tFGFR1 and SH3BP2 in SA cells expressing an SH3BP2 shRNA (E) or overexpressing SH3BP2 (F). **G**, Co-immunoprecipitation analysis. Left, the FGFR1 immunoprecipitate was immublotted for SH3BP2. Right, the SH3BP2 immunoprecipitate was immunoblotted for FGFR1. The levels of the proteins in the input are shown. **H**, Soft agar colony formation assay. NIH 3T3 cells expressing a NS shRNA or one of two unrelated SH3BP2 shRNAs were analyzed for their ability to form colonies in soft agar. **I**, Tumor formation in mice injected with NIH 3T3 cells

expressing a NS shRNA or one of two unrelated SH3BP2 shRNAs. **J**, Model depicting the mechanism by which loss of SRSF9 leads to increased FGFR1 levels. **K**, Boxplots displaying log2 fold changes in expression of *SH3BP2* exon 10 in normal lung samples, 27 hLSCC samples and 10 human lung adenocarcinoma (hLA) samples. Boxed areas span the first to the third quartile. Whiskers represent 15^{th} and 85^{th} percentiles. $P<0.05$ for hLSCC versus hLA. *$P<0.05$; **$P<0.01$.

Table 1

List of 32 candidate TSGs validated in mouse tumorigenesis and soft agar colony formation assays.

Biological process	Gene symbol	Gene name	Human homolog
Cell signaling	*Angpt1*	angiopoietin 1	*ANGPT1*
	Dapp1	dual adaptor for phosphotyrosine and 3-phosphoinositides 1	*DAPP1*
	Fpr3	formyl peptide receptor 3	*FPR3*
	Gapvd1	GTPase activating protein and VPS9 domains 1	*GAPVD1*
	Igf2r	insulin-like growth factor 2 receptor	*IGF2R*
	Myd88	myeloid differentiation primary response gene 88	*MYD88*
	Pkd1l3	polycystic kidney disease 1 like 3	*PKD1L3*
	Prl7a2	prolactin family 7, subfamily a, member 2	–
	Ptpn4	protein tyrosine phosphatase, non-receptor type 4	*PTPN4*
	Stk11	serine/threonine kinase 11	*STK11*
Cell growth/migration/metabolism	*Cdk5r1*	cyclin-dependent kinase 5, regulatory subunit 1 (p35)	*CDK5R1*
	Flna	filamin, alpha	*FLNA*
	Map1a	microtubule-associated protein 1 A	*MAP1A*
	Nme4	non-metastatic cells 4, protein expressed in	*NME4*
	Sema3b	sema domain, immunoglobulin domain (Ig), short basic domain, secreted, (emaphoring) 3B	*SEMA3B*
	Slfn4	schlafen 4	–
	Spast	spastin	*SPAST*
DNA/RNA metabolism	*Ddx52*	DEAD (Asp-Glu-Ala-Asp) box polypeptide 52	*DDX52*
	Naa38	LSM8 homolog, U6 small nuclear RNA associated (*S. cerevisiae*)	*NAA38*
	Orc1	origin recognition complex, subunit 1-like (*S. cerevisiae*)	*ORC1*
	Srsf9	splicing factor, arginine/serine rich 9	*SRSF9*
Immunity	*Cr1l*	complement component (3b/4b) receptor 1-like	–
	Gzma	granzyme A	*GZMA*
Lipid metabolism	*Pigh*	phosphatidylinositol glycan anchor biosynthesis, class H	*PIGH*
	Ptgis	prostaglandin I2 (prostacyclin) synthase	*PTGIS*
Nuclear transport	*Nup205*	nucleoporin 205	*NUP205*
Transcriptional regulation	*Spop*	speckle-type POZ protein	*SPOP*
	Zfp422	zinc finger protein 422	*ZNF22*
Protein folding/export/metabolism	*Dnajc12*	DnaJ (Hsp40) homolog, subfamily C, member 12	*DNAJC12*
	Sdf2l1	stromal cell-derived factor 2-like 1	*SDF2L1*
	Txnrd1	thioredoxin reductase 1	*TXNRD1*
Unknown	*Wap*	whey acidic protein	–